Vincent Methot*, Patricia Ulloa and Martin A. Koch

Pore size estimation from double diffusion encoding

A multidimensional acquisition helps reduce numerical inversion instability

Abstract: Double diffusion encoding is a magnetic resonance technique with applications in measuring microstructure. In many tissues, cell size (which is of a few micrometers) is an important biological parameter. Estimating an arbitrary pore size distribution from a diffusion attenuated signal usually relies on varying a single experimental setting. This inversion process is numerically unstable. Numerical simulations are presented, where multiple experimental settings are varied concomitantly. The inversion's results show good agreement with ground truth.

Keywords: diffusion MRI, double diffusion encoding, DDE, numerical simulation, pore size estimation

https://doi.org/10.1515/cdbme-2017-0131

1 Introduction

Axonal diameter is an index of importance when trying to understand the complex structure and functions of the central nervous system. This measure has an impact on conduction speed in the brain [1, 2], which itself affects brain behaviour [3, 4]. Axonal diameter is also closely linked with aging [5] and certain neuropathologies [6, 7]. Non-invasive estimation of the axonal diameter distribution in the human brain is nonetheless limited to specific anatomical regions, due to technical difficulties like orientation dispersion and limited gradient strength [8, 9] as well as acquisition time [10]. In this context, we explore, via numerical simulations, the possibility to use double diffusion encoding (DDE) [11] to attain clinically feasible pore size estimation (see **Figure 1** for a schematic representation of the effective gradient waveform of DDE).

Originally aimed at measuring pore size and shape [12, 13], DDE is an emerging diffusion magnetic resonance imaging (MRI) technique. Recent advances in the analytical description of the diffusion MRI signal [14], as well as its numerical prediction [15, 16], make it now conceivable to study and optimize the sensitivity of this experimental protocol. Previous work [17] has shown that the parallel-antiparallel difference in signal attenuation in DDE decays exponentially with an increase of delay between diffusion encodings – the mixing time (τ_m). This decay depends on the pore size. The phenomenon can theoretically even be observed in unaligned structures like crossing fibres in the brain. A pore size distribution (PSD) can then be estimated with the numerical Laplace transform inversion [17], which is unstable [18]. Tikhonov regularization and a non-negativity constraint improve the procedure, making it possible to recover a simple PSD. Nonetheless, this method's results are not encouraging for the study of complex arbitrary distributions often present in biological systems, the regularization term flattening the reconstructed PSD considerably.

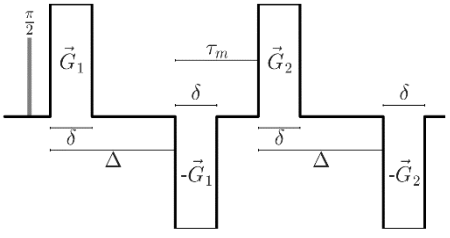

Figure 1 – Effective diffusion gradient waveform of the DDE experiment with its timing parameters. Ψ is the angle between $\vec{G}_1$ and $\vec{G}_2$.

DDE is controlled via many experimental parameters (see **Figure 1** - two durations (δ), amplitudes (G) and orientations, diffusion times (Δ) and mixing time (τ_m). We present here the use of supplementary variables to stabilize the numerical inversion. A multidimensional DDE experiment could reduce the instability of the inversion process [19].

***Corresponding author: Vincent Methot:** Institute of Medical Engineering, University of Luebeck, Ratzeburger Allee 160, 23562 Lübeck, Germany, e-mail: methot@imt.uni-luebeck.de
Patricia Ulloa, Martin A. Koch: Institute of Medical Engineering, University of Luebeck, Ratzeburger Allee 160, 23562 Lübeck, Germany, e-mail: {ulloa, koch}@imt.uni-luebeck.de

2 Method

The general idea of the present contribution is to simulate, for a known, arbitrary PSD and many different experimental settings, the expected signal attenuation due to diffusion. The attenuation, for the same set of experimental parameters, is also simulated for pores of all single diameters individually. The inversion process involves finding the best distribution of pores of single diameter which can explain the attenuation signal simulated for the arbitrary PSD.

All numerical simulations were calculated using the MISST v0.93 [16, 20, 21] package run on Matlab2016b (Palo Alto, CA). A spherical pore model was chosen, as well as the experimental parameters shown in **Table 1**. Both diffusion encodings were similar ($\delta_1 = \delta_2 = \delta$, $\Delta_1 = \Delta_2 = \Delta$, $||\overrightarrow{G_1}|| = \left|\left|\overrightarrow{G_2}\right|\right| = G$) except for their orientation. In our case, only the relative angle between G_1 and G_2 (Ψ) is relevant.

Table 1: Simulation parameters in MISST

Parameter	Min : Increment : Max	Unit
Diameter (d)	5 : 0.5 : 20	µm
Mixing time (τ_m)	δ / ms : 1 : δ / ms + 50	ms
Gradient duration (δ)	4 : 1 : 24	ms
Diffusion time (Δ)	δ / ms : 1 : δ / ms + 50	ms
Angle between encodings (Ψ)	0 : π/8 : 2π	rad
Diffusion coefficient (D_0)	2	$\mu m^2 ms^{-1}$
Gradient strength (G)	45	$mT\ m^{-1}$

For every combination of parameters, all PSD's expected signal attenuation (within the limits of the simulated pore sizes) were composed by a weighted sum of attenuation values from single pore size's diffusion attenuation. **Table 2** lists the subset of PSDs under scrutiny in the current study. Single pore size and mixtures of Gaussian distributions were chosen for their simplicity and versatility; the gamma distribution for its frequent usage in biological models. Gaussian noise was then added to mimic a signal-to-noise ratio of 100 for the non-diffusion weighted image. Inversion was done using non-negative least-squares with Tikhonov regularization (regularization parameter λ).

Table 2: PSDs under scrutiny.

Location	Distribution type	Mean / µm	Variance / µm
Figure 2a	Single diameter	9	
Figure 2b	Gaussian	7	2
Figure 2c	2x Gaussian	7, 17	2
Figure 2d	Gamma	10	5
Figure 3a	Gaussian	17	1
Figure 3b	Gaussian	7	1
Figure 3c	2x Gaussian	7, 17	1, 1
Figure 3d	2x Gaussian	7, 17	1, 0.5

3 Results

Results are shown in **Figure 2** and **Figure 3**. In both cases, the green line shows the initially simulated PSD while the red bars represent the estimation from the numerical inversion. **Figure 2** shows the fidelity of the inversion for different PSDs. **Figure 3** shows the efficiency of the same inversion procedure, but for different mixtures of Gaussian distributions.

4 Discussion

The results shown here, as well as supplementary PSDs tested concomitantly, suggest good agreement between initial and estimated distributions, especially with the relatively low SNR of 100. A higher SNR generally relaxed the necessity of regularization (meaning using a lower λ, which normally leads to less smoothing), but without visibly improving the accuracy of the estimate. A lower SNR normally led to poor PSD estimation, even at stronger regularization.

From **Figure 2** and **Figure 3**, we can see that the estimated distribution is slightly shifted to higher diameters. This might be due to an intrinsic limitation of diffusion MRI in estimating pore size [22]. Small pores are harder to estimate, with an experimental limit around 5 µm at 45 mT m^{-1}. Estimating PSDs constituted of larger pores (>10mm) proves herein more accurate, even without regularization, than one with smaller pores.

Although pore size can be estimated from experiments individually by varying τ_m, δ, Δ or Ψ, we show that there is significant advantage to vary conjointly multiple parameters, as proposed in [23], thus rendering the inversion process more stable. This is useful when estimating, without prior model, the complete PSD. Such an estimation might even be possible at limited clinical gradient strength with realistic acquisition time [24]. Our method, although still using values from a vast parameter space, promises a considerable acceleration from a more intelligent sampling. The capacity to calculate in advance, for any pore diameter, the result of a DDE experiment with arbitrary parameters, makes it possible to select a multidimensional subset with optimal contrast after the inversion (see [25] for an inspiring example).

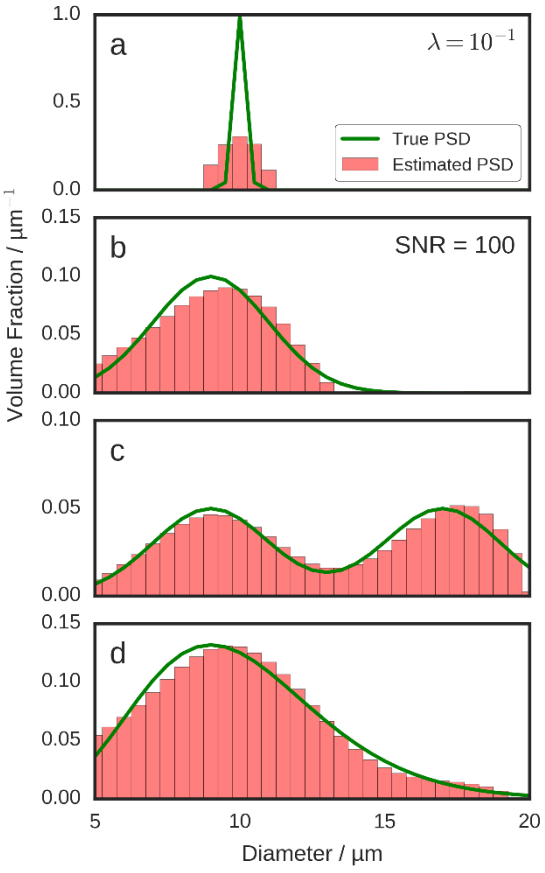

Figure 2 – Inversion results for different PSDs. The green line represents the simulated distributions and represents the ground truth, for assessing the quality of the inversion. Red histograms are the results of the inversion process. Distribution characteristics can be found on Table 2.

Finally, before tackling the estimation of fiber axonal diameter distribution in the brain, at least two more aspects need to be accounted for: (1) estimation of cylinder diameters will require a different acquisition scheme, taking into consideration the absolute orientation of both diffusion encodings (4 degrees of freedom) instead of only the relative angle between the two (1 degree of freedom). Efficient strategies have already been proposed to reduce the related supplementary amount of data, and hence the acquisition time [26]. (2) An experiment in biological systems will need to account for free diffusion and variations in the diffusion coefficient. The brain, *e.g.*, usually has a large extracellular water fraction, which makes pore size distribution more difficult. Even higher SNR would therefore be necessary.

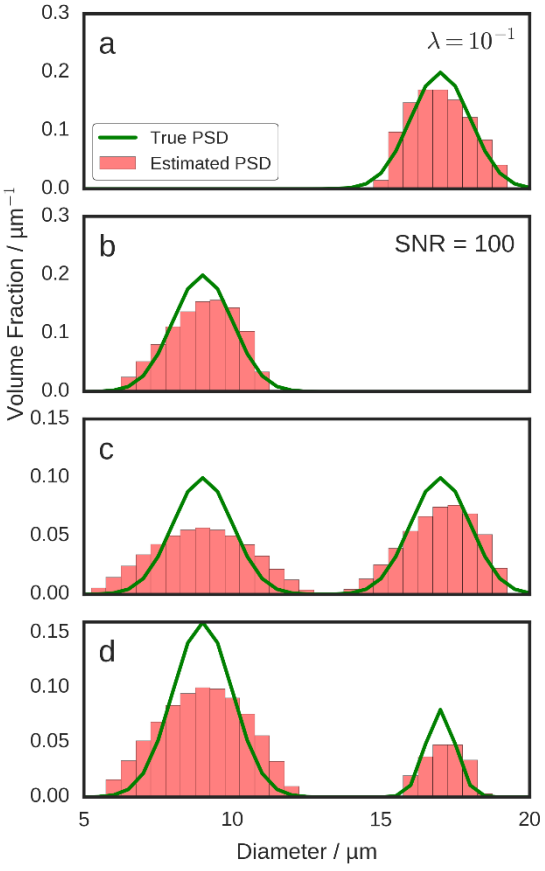

Figure 3 – Inversion results for different Gaussian PSDs. As in Figure 2, the green line represents the simulated distributions and red histograms are the results of the inversion process. Distribution characteristics can be found in Table 2.

5 Conclusion

The DDE experiment offers more degrees of freedom than single diffusion encoding. We numerically studied a set of timing parameters to be varied (τ_m, δ, Δ, Ψ). The proposed inversion process renders good PSD estimation between 5 µm and 20 µm without requiring strong regularization.

Translation to an *in vitro* study, using a clinical scanner, although not straightforward, seems to be attainable.

Author's Statement

Research funding: Patricia Ulloa was supported by the Graduate School for Computing in Medicine and Life Sciences funded by Germany's Excellence Initiative [DFG GSC 235/2-1] and [DFG KO 3389/2-1]. Conflict of interest: Authors state no conflict of interest. Informed consent: Informed consent is not applicable. Ethical approval: The conducted research is not related to either human or animals use

References

[1] J. M. Ritchie. Proc. R. Soc. B Biol. Sci., vol. 217, pp. 29–35, Dec. 1982.
[2] S. G. Waxman. Muscle Nerve, vol. 3, pp. 141–150, Mar. 1980.
[3] J. L. Ringo, R. W. Doty, S. Demeter, and P. Y. Simard. Cereb. Cortex, vol. 4, pp. 331–43.
[4] J. A. McNab, B. L. Edlow, T. Witzel, S. Y. Huang, H. Bhat, K. Heberlein, T. Feiweier, K. Liu, B. Keil, J. Cohen-Adad, M. D. Tisdall, R. D. Folkerth, H. C. Kinney, and L. L. Wald. Neuroimage, vol. 80, pp. 234–245, 2013.
[5] L. Marner, J. R. Nyengaard, Y. Tang, and B. Pakkenberg. J. Comp. Neurol., vol. 462, pp. 144–152, 2003.
[6] G. Lovas, N. Szilágyi, K. Majtényi, M. Palkovits, and S. Komoly. Brain, vol. 123, pp. 308–317, 2000.
[7] S. Cluskey and D. B. Ramsden. Mol. Pathol., vol. 54, pp. 386–92, Dec. 2001.
[8] Y. Assaf, T. Blumenfeld-Katzir, Y. Yovel, and P. J. Basser. Magn Reson Med, vol. 59, pp. 1347–1354, Jun. 2008.
[9] D. C. Alexander, P. L. Hubbard, M. G. Hall, E. a. Moore, M. Ptito, G. J. M. Parker, and T. B. Dyrby. Neuroimage, vol. 52, pp. 1374–1389, 2010.
[10] D. Benjamini, M. E. Komlosh, L. A. Holtzclaw, U. Nevo, and P. J. Basser. Neuroimage, vol. 135, pp. 333–344, 2016.
[11] N. Shemesh, S. N. Jespersen, D. C. Alexander, Y. Cohen, I. Drobnjak, T. B. Dyrby, J. Finsterbusch, M. A. Koch, T. Kuder, F. Laun, M. Lawrenz, H. Lundell, P. P. Mitra, M. Nilsson, E. Özarslan, D. Topgaard, and C.-F. C.-F. Westin. Magn. Reson. Med., vol. 75, pp. 82–87, Jan. 2016.
[12] P. P. Mitra. Physical Review B, vol. 51, pp. 15074–15078, 1995.
[13] Y. Cheng and D. G. Cory. J. Am. Chem. Soc., vol. 121, pp. 7935–7936, 1999.
[14] E. Özarslan and P. J. Basser. J. Chem. Phys., vol. 128, p. 154511, 2008.
[15] P. T. Callaghan. J. Magn. Reson., vol. 129, pp. 74–84, 1997.
[16] I. Drobnjak, H. Zhang, M. G. Hall, and D. C. Alexander. J. Magn. Reson., vol. 210, pp. 151–157, 2011.
[17] V. Methot and M. A. Koch. Proc. 33rd annual meeting ESMRMB #173 (2016).
[18] C. L. Epstein and J. Schotland. SIAM Rev., vol. 50, pp. 504–520, 2008.
[19] D. Benjamini and U. Nevo. J. Magn. Reson., vol. 230, pp. 198–204, 2013.
[20] I. Drobnjak, B. Siow, and D. C. Alexander. J. Magn. Reson., vol. 206, pp. 41–51, 2010.
[21] A. Ianuş, B. Siow, I. Drobnjak, H. Zhang, and D. C. Alexander. J. Magn. Reson., vol. 227, pp. 25–34, 2013.
[22] Nilsson, M., Lasič, S., Drobnjak, I., Topgaard, D. & Westin, C.-F.. NMR Biomed. e3711 (2017).
[23] Benjamini, D., Komlosh, M. E., Basser, P. J. & Nevo, U.. J. Magn. Reson. 246C, 36–45 (2014).
[24] Katz, Y., Benjamini, D., Basser, P. J. & Nevo, U.. Proc. 23rd Annual Meeting ISMRM, Toronto, Canada #2771 (2015).
[25] Benjamini, D. & Basser, P. J.. Microporous Mesoporous Mater. (February 2017).
[26] Jespersen, S. N., Lundell, H., Sønderby, C. K. & Dyrby, T. B.. NMR Biomed. 26, 1647–1662 (2013).